

Cascade switching current detectors based on arrays of Josephson junctions

Roger Cattaneo,¹ Artemii E. Efimov,^{1,2} Kirill I. Shiiyanov,¹ Oliver Kieler,³ and Vladimir M. Krasnov^{1,*}

¹*Department of Physics, Stockholm University, AlbaNova University Center, SE-10691 Stockholm, Sweden.*

²*Department of Physics, University of Basel, 4056 Basel, Switzerland*

³*Physikalisch-Technische Bundesanstalt, 38116 Braunschweig, Germany*

Cascade multiplication is a common technique to enhance the sensitivity of photon detectors. In this study, we demonstrate novel cascade-amplified superconducting detectors utilizing arrays of Josephson junctions. The mutual coupling between junctions induces avalanche-like switching of multiple junctions upon photon absorption, leading to cascade amplification of the readout voltage. We present two prototypes featuring either low- T_c linear Nb/Nb_xSi_{1-x}/Nb arrays, or high- T_c stacked intrinsic Josephson junctions. Both devices exhibit clear antenna effects in microwave directivities, indicating good impedance matching and absorption efficiency. The combination of high absorption efficiency and large cascade amplification has the potential to produce broadband THz sensors with sensitivity exceeding 10^{13} V/W.

INTRODUCTION

THz detectors find diverse applications, including security, environmental monitoring, medical imaging, chemical analysis, and fundamental research [1–4]. Cooling to cryogenic temperatures improves detector sensitivity by reducing thermal noise and background radiation. Ultra-sensitive cryogenic detectors based on semiconductors [5], graphene [6], and superconductors [7] have been demonstrated. Superconductors are particularly well suited for THz detection because their characteristic energies (Josephson energy, superconducting gap, etc.) are naturally placed in the THz range and could be easily tuned for achieving optimal operation [8].

A Josephson junction (JJ) can act as a sensitive switching current detector (SCD) with a potential for single-photon resolution in a broad microwave (MW) to THz range [8–23]. When JJ is biased just below the critical current, $I \lesssim I_c$, a small-amplitude electromagnetic signal triggers its switching from the superconducting to the resistive state. The responsivity of SCD can be very high, limited only by quantum fluctuations [8, 24]. The upper frequency depends on the characteristic voltage, $V_c = I_c R_n$, and ranges from sub-THz for low- T_c [12], to THz for high- T_c [19, 21, 22, 25] JJs. The highest $V_c \gtrsim 30$ mV [26, 27] is achieved in intrinsic Josephson junctions (IJJs), naturally occurring in Bi₂Sr₂CaCu₂O_{8+δ} (Bi-2212) cuprates [28]. Operation of IJJs above 10 THz has been demonstrated [19, 25]. The atomic-scale of IJJs enables strong mutual coupling, advantageous for the creation of coherent THz sources [19, 22, 29–35].

Cascade multiplication is widely employed for enhancing detector sensitivity, e.g. in photo-multipliers and avalanche photodiodes [4]. For Josephson detectors, this could be achieved using arrays of mutually coupled JJs. The coupling leads to a current-locking phenomenon [36], where the switching of one JJ drags several neighbors into the resistive state, thereby multiplying the readout volt-

age [36–38]. A good detector should also have a high absorption efficiency, defined as the ratio of absorbed to incoming THz power. This necessitates impedance matching with free space, which is equally important for both THz sources and sensors [35, 39–41].

In this work we demonstrate novel types of cascade-amplified SCDs featuring arrays of coupled JJs. Collective, avalanche-like switching of many JJs leads to cascade amplification of the readout voltage, boosting the SCD sensitivity. We present two prototypes based on either linear arrays of low- T_c Nb/Nb_xSi_{1-x}/Nb JJs or stacked high- T_c IJJs in Bi-2212 whisker-type crystals. We investigate both MW and THz responses and observe non-trivial MW directivities, manifesting antenna effects associated with the sample geometry. This suggests good impedance matching and absorption efficiencies for both types of devices. We argue that the combination of high- T_c superconductivity with high absorption efficiency and large cascade gain can yield broadband THz sensors with outstanding sensitivities.

RESULTS

JJ arrays can be advantageously used for photon detection. It has been shown that utilization of arrays can help in impedance matching and broaden the detector range [42, 43]. However, earlier studies were focusing on heterodyne mixers, operating at the quasiparticle branch of the current-voltage (I - V) characteristics. In contrast, here we consider SCD, where the signal is generated upon switching out of the superconducting state [8–23].

Our goal is to achieve cascade amplification of the readout voltage. Individual JJs inherently exhibit variations. Without interjunction coupling, the array I - V is simply the sum of independent JJ I - V 's. However, when the coupling is present, a current-locking phenomenon may occur [36], causing all (or several) JJs to switch simultaneously. Such collective switching leads to a cascade multiplication of the readout voltage, proportional to the number of current-locked JJs [36–38]. The effi-

* Vladimir.Krasnov@fysik.su.se

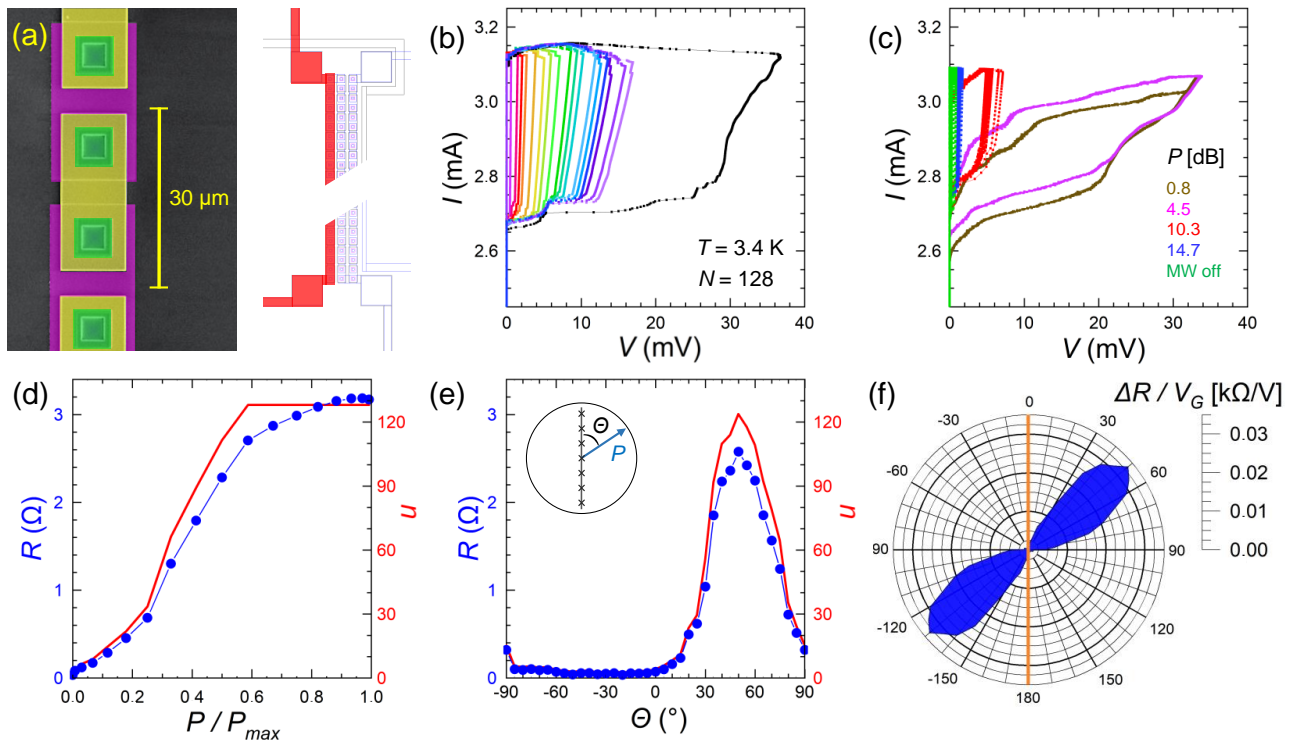


FIG. 1. **Cascade SCD based on a linear Nb/Nb_xSi_{1-x}/Nb array.** (a) SEM image (left, false color) and layout (right) of the array. The studied line is marked in red. (b) Ensemble of the I - V 's without MW irradiation, obtained at slightly different bias currents. (c) The I - V 's with a fixed bias amplitude for different MW powers at $f \simeq 74.5$ GHz. Switching of multiple JJs leads to cascade amplification of the readout voltage. (d) The lock-in resistance of the array, R , (blue symbols, left axis) and the number of active JJs, n , (red line, right axis) as a function of MW power. (e) R and n as a function of the polarization angle, Θ , for $P = \text{const}$. (f) Angular diagram of detector sensitivity. The orange line marks the orientation of the array. A profound off-axis directivity manifest the traveling-wave antenna effect.

ciency of cascading depends on the uniformity of JJs and the strength of coupling. Therefore, arrays with many strongly interacting JJs are required to achieve high gain.

Microwave detection

A linearly polarized MW signal at $f \simeq 74.5$ GHz is delivered to the sample in a quasi-optical manner. MW attenuation and polarization angle are adjusted using grid polarizers. The incoming MW power, P , is monitored by a Golay cell. Experimental details can be found in the Supplementary. All presented measurements are performed at zero magnetic field and $T \simeq 3.3$ K.

Linear Nb arrays

Fig. 1 (a) shows a scanning electron microscope (SEM) image and a layout of a Nb/Nb_xSi_{1-x}/Nb array. We study a linear section (marked red) with $N = 128$ JJs. Details about fabrication and characterization of the arrays can be found in Refs. [44–47]. Fig. 1 (b) shows the I - V 's measured upon minor variation of the bias current amplitude, I_b , in the absence of MW. Multiple branches

correspond to a different number, n , of active JJs. Inter-junction coupling in these arrays is mediated by surface plasmons [46]. Such traveling waves are manifested by the appearance of collective resonant steps in the I - V 's [47]. The largest step is clearly visible in the rightmost (black) I - V in Fig. 1 (b) with all $N = 128$ active JJs.

Fig. 1 (c) shows a set of the I - V 's measured at a fixed I_b for different MW powers. With increasing P , the switching current, I_s , decreases and progressively more JJs switch into the resistive state, leading to increasing of the readout voltage. Blue symbols and the red line in Fig. 1 (d) represent the lock-in resistance of the array, R , and the number of active JJs, n , respectively. It can be seen that the rapid increase of R at low P is proportional to n , illustrating the cascade amplification phenomenon. At high power, when all $N = 128$ JJs are in the resistive state, the responsivity dR/dP is greatly reduced. In this case the response is solely due to the decrease of $I_s(P)$, qualitatively similar to a single-JJ SCD [8, 19]. Thus the large difference in low and high- power responsivities highlights the advantage of array-based cascade SCD compared to a conventional single-JJ SCD.

A sensitive detector should efficiently absorb the incoming power. The optimal absorption (and emission) efficiency (50 %) is achieved at the impedance matching

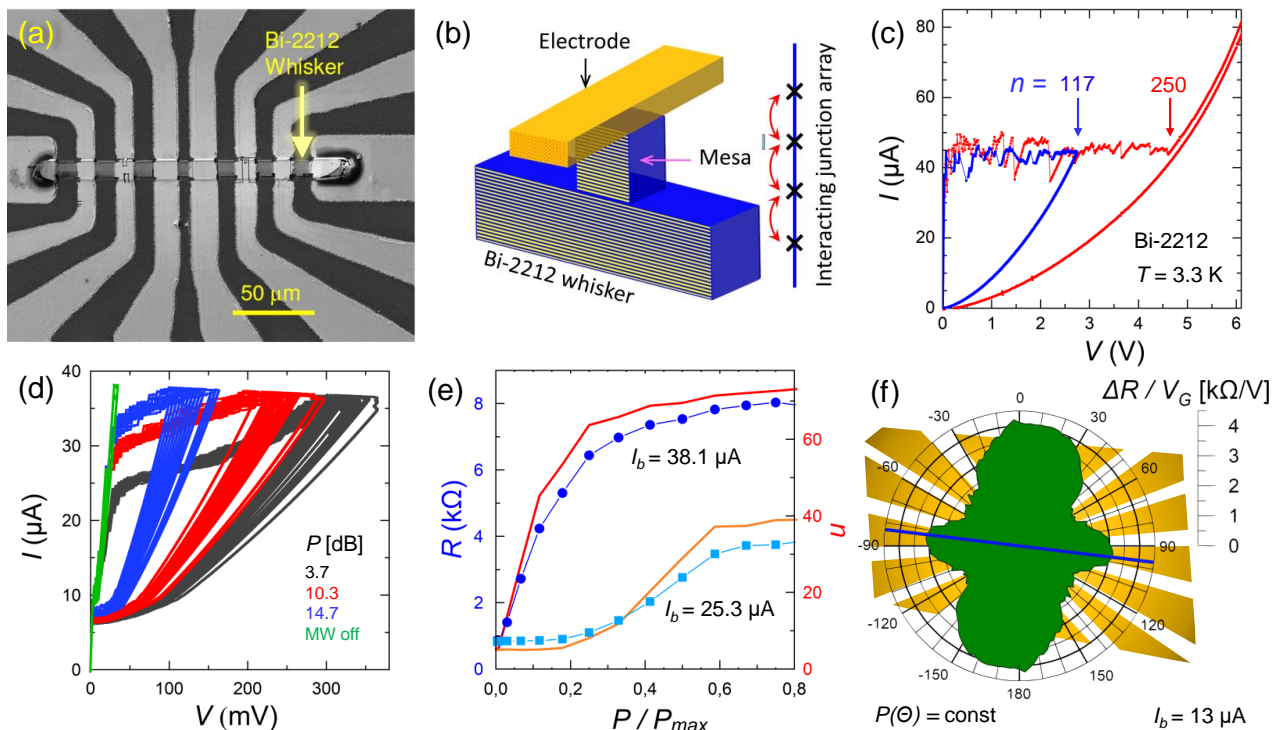


FIG. 2. **Microwave characteristics of a Bi-2212 mesa.** (a) A SEM image of a whisker-based device. (b) Sketch of a mesa formed at the intersections of the whisker with a top Au-electrode. It has a turnstile antenna geometry. (c) Two I - V s of a mesa with $N = 250$ IJJs, in the absence of MW. (d) Ensemble of the I - V s for different MW powers at $I_b = 38.1 \mu\text{A}$. (e) The mesa resistance (symbols) and the number of active IJJs, n , (lines) versus the MW power, for $I_b = 25.3$ and $38.1 \mu\text{A}$. (f) The directivity diagram. The blue line indicates the orientation of the whisker. The yellow background shows the large-scale electrode geometry. The four-fold directivity is consistent with the turnstile-antenna geometry of the device.

condition [39–41]. A JJ alone cannot effectively absorb radiation because its size is much smaller than the wavelength of radiation in free space, λ_0 , [39]. Therefore, mm-long electrodes play a crucial role as impedance matching antennas [35]. The presence or absence of geometry-specific antenna effects provides a clue about the effectiveness of impedance matching and MW absorption.

The active part of Nb-array is about 2 mm long ($\sim \lambda_0/2$ at 74.5 GHz). Additionally, there are long passive electrodes (without JJ) with a total length ~ 1 cm. These long electrodes may act as non-resonant traveling wave antennas, which are characterized by asymmetric off-axis directivities [45, 46]. Fig. 1 (e) shows the array resistance (blue symbols) and the number of active JJs (red line) as a function of the polarization angle, Θ , at a constant P . $\Theta = 0$ corresponds to the MW electric field parallel to the array line. Fig. 1 (f) displays the corresponding sensitivity diagram, $\Delta R/V_G(\Theta)$, where ΔR is the resistance increase with respect to the turned-off MW, and $V_G \propto P$ is the Goly cell voltage (constant in this experiment). The diagram exhibits two lobes with a large directivity at $\Theta \simeq 50^\circ$ with respect to the array. Such off-axis directivity indicates traveling-wave antenna operation of long electrodes, enabling good impedance matching and absorption efficiency.

Mesa structures on Bi-2212 whiskers

Figure 2 (a) shows a SEM image of one of the studied high- T_c devices. They are based on Bi-2212 whiskers - needle like single crystals [22]. Each device contains several mesas, representing stacks of IJJs. Mesas are formed at the intersection of the whisker with top gold electrodes, as sketched in Fig. 2 (b). To reduce the I_c and increase the sensitivity, some mesas were trimmed using focused ion beam (FIB) etching [19, 48]. Details about sample fabrication and characterization can be found in Refs. [19, 22, 35, 48] and the Supplementary.

Fig. 2 (c) displays two I - V 's of a mesa ($\sim 5 \times 5 \mu\text{m}^2$), containing $N \simeq 250$ IJJs, without MW. The blue curve, with $n = 117$ active IJJs, is measured with I_b slightly above the mean switching current, $I_s^* \sim 50 \mu\text{A}$. A multi-branch structure ends at $V \simeq 5$ V when all $N \simeq 250$ IJJ's switch into the resistive state (red curve). The large readout voltage is caused by the large $V_c \simeq 20$ mV per IJJ. Switching of the first and the last IJJ occurs within an interval, $\sigma \sim 5 \mu\text{A} \sim 0.1 I_s^*$, representing the width of the switching current distribution [8, 49]. By varying I_b in this narrow range, we can continuously tune n from 1 to 250. The responsivity of SCD is determined by the effective differential resistance, $R_d = dV/dI$, in

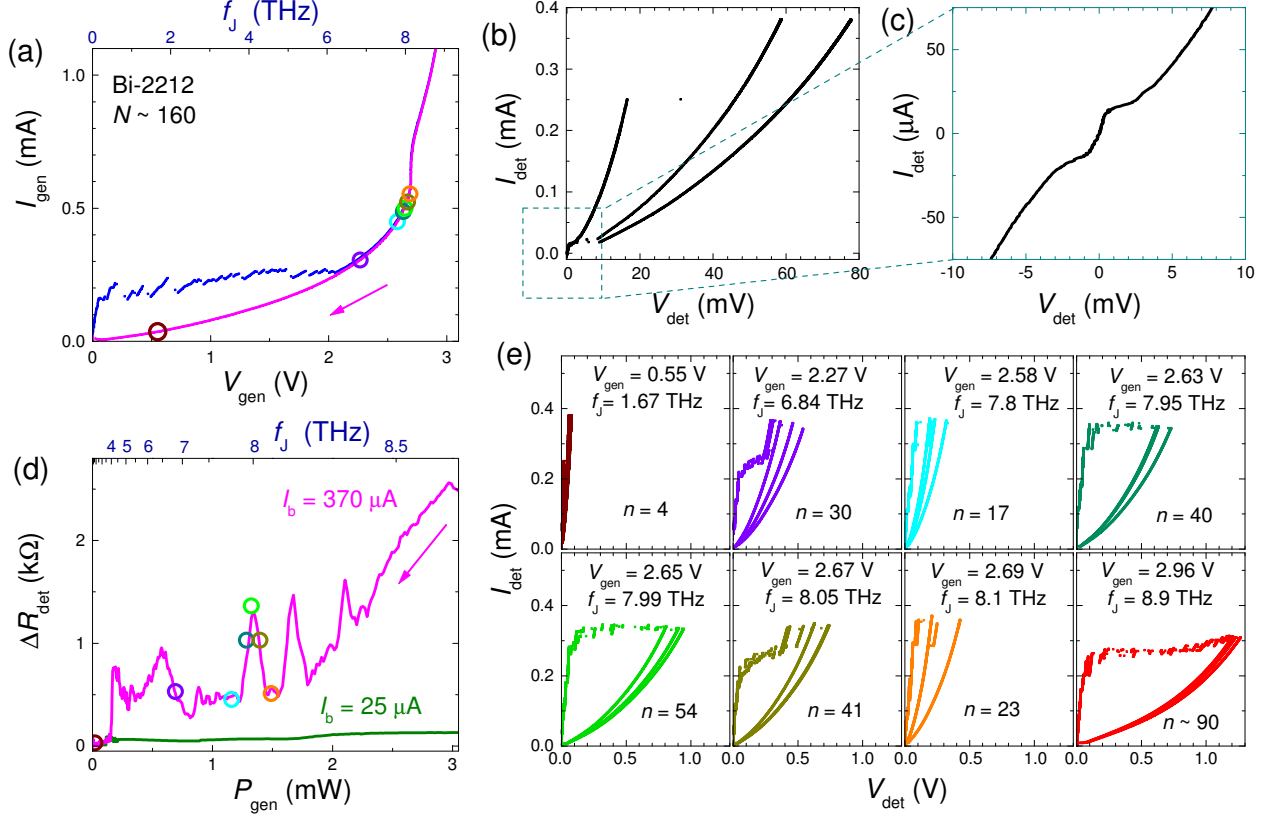


FIG. 3. **Detection of THz radiation from a Bi-2212 mesa.** (a) The I - V of the generator mesa for upward (blue) and downward (magenta) bias sweeps. Top axis indicates the anticipated Josephson frequency. (b) and (c) Low-bias I - V 's of the detector mesa with (c) representing the I - V of the weak surface junction. (d) Measured detector responses versus $P_{gen} = I_{gen}V_{gen}$. The olive line is obtained with $I_b = 25 \mu\text{A}$, activating only a single surface IJJ. The magenta curve is measured with $I_b = 370 \mu\text{A}$, activating many IJJs. (e) A set of detector I - V 's with $I_b = 370 \mu\text{A}$ at different bias points of the generator, marked by the same-color circles in (a) and (d). It can be seen that the cascade amplification factor, n , is playing the dominant role in boosting the detector sensitivity.

the switching region [9]. For this mesa it is very large, $R_d = NV_c/\sigma \sim 1 \text{ M}\Omega$, as a consequence of the cascading.

Fig. 2 (d) shows the I - V s of another mesa at different MW powers and $I_b = 38.1 \mu\text{A}$. The cascade gain depends on bias. Fig. 2 (e) represents the MW power dependencies of R (symbols) and n (lines), measured at two biases. At lower $I_b = 25.3 \mu\text{A}$, the sensitivity, dR/dP , remains small up to some threshold, $P \sim 0.2 P_{max}$. At higher $I_b = 38.1 \mu\text{A}$, there is no threshold and the sensitivity is high at $P = 0$. With further increase of I_b , the sensitivity remains high at $P = 0$ but saturates at successively smaller P , thus reducing the dynamic range [8]. Therefore, there is an optimal bias ($I_b = 38.1 \mu\text{A}$ in this case) with both high sensitivity and large dynamic range. For comparison, in the Supplementary we analyze the ordinary SCD operation on the same mesa using a single surface IJJ. The surface IJJ has much smaller I_s [27] and can be measured without activation of other IJJs [19]. The maximum single-junction response is $\Delta R \sim 40 \Omega$, much smaller than $\sim 8 \text{ k}\Omega$ for the cascade SCD in Fig. 2 (e) at the same MW power for the same mesa.

Fig. 2 (f) shows the MW directivity of this mesa. It exhibits a four-fold shape. The two smaller lobes are aligned with the whisker (indicated by the blue line). The larger lobes are approximately perpendicular, slightly inclined in the direction of one of bias electrodes (see the Supplementary for more details). The large-scale electrode geometry of this device is shown in the background (yellow). The observed four-fold directivity is consistent with the whisker-mesa-electrode geometry, which form a turnstile-antenna, as shown in Fig. 2 (b) [50].

Detection of THz radiation from a Bi-2212 mesa

To verify THz operation, we perform an in-situ generation-detection experiment in which one Bi-2212 mesa emits Josephson radiation and a nearby mesa detects it [19, 22]. Fig. 3 (a) shows the I - V of a generator mesa ($\sim 10 \times 15 \mu\text{m}^2$), containing $N = 160 \pm 10$ IJJs. We analyze the downturn part of it (magenta) at which all N IJJs are active. In this case, the Josephson frequency is

well defined, $f_J = 2eV/hN$, as indicated in the top axis. Emission from Bi-2212 mesas occurs at cavity modes inside the mesa [19, 32, 33]. The key signature of such emission (as opposed to heating) is the non-monotonous dependence on the dissipation power, $P_{\text{gen}} = I_{\text{gen}}V_{\text{gen}}$, with distinct peaks at cavity resonances [19].

Fig. 3 (b) shows a low-bias part of the I - V of a detector mesa ($\sim 15 \times 15 \mu\text{m}^2$), about $22 \mu\text{m}$ away from the generator mesa. Fig. 3 (c) is a close-up on the central part, representing the I - V of the surface junction. It has $I'_c \simeq 15 \mu\text{A}$, significantly smaller than $I_c \simeq 370 \mu\text{A}$ for the rest of the IJJs. This disparity allows ordinary SCD measurements at $I'_c < I_b \ll I_c$, which activates only one surface IJJ [19]. The cascade SCD can be analyzed on the same mesa by increasing bias to $I_b \gtrsim I_c$.

Fig. 3 (d) shows single-junction (olive) and cascade (magenta) SCD responses versus P_{gen} , measured at bias amplitudes, $I_b = 25$ and $370 \mu\text{A}$, respectively. It can be seen that (in this case) the resolution of a single-junction SCD is not sufficient for resolving the emission. The cascade SCD demonstrates a much larger response with clearly visible emission peaks. The main emission for this generator mesa occurs in the range from ~ 4 to 8.4 THz, as indicated by the top axis in Fig. 3 (d). Fig. 3 (e) shows the detector I - V 's measured with $I_b = 370 \mu\text{A}$ at several bias points of the generator, marked by the same-color circles in Figs. 3 (a) and (d). It can be seen that cascade amplification factor, n , is playing the dominating role in the detector response.

DISCUSSION

We observed similar behavior both for low- and high- T_c devices, either linear arrays or stacks. Both types of detectors have some advantages. 2D-linear arrays facilitate a large absorption area and a simple scalability to tens of thousand of JJs [44].

The list of advantages of high- T_c devices include: (i) Broad frequency range covering the whole THz area [0.1-10] THz [19]. (ii) Compactness in combination with large N . (iii) Large $V_c \sim 20 - 30$ mV [26, 27], enabling high readout signals. From Figs. 1 (b) and 2 (c) it can be seen that the maximum readout voltage, NV_c , for a high- T_c mesa (5 V) is more than 100 times larger than for a low- T_c array (~ 0.04 V) despite only a factor two difference in N (250 vs. 128). (iv) The atomic separation of IJJs enables the strongest interjunction coupling, needed for the avalanche switching.

Sensitivity of a cascade SCD

As described in the Supplementary, for Bi-2212 detector the maximum sensitivity, $\Delta R/V_G$, increases from 0.37 k Ω/V for the conventional single junction SCD (no amplification, $n = 1$), 18 k Ω/V at sub-optimal bias, and up

to 100 - 120 k Ω/V at the optimal bias, Fig. 2 (e). We emphasize that these measurements were performed under the same conditions with the only difference in the bias amplitudes, which determine the cascade amplification.

The detector sensitivity $S(V/W)$ can be calculated in the following way. The readout voltage from the array is $V(n) = nV_c$. The spread of switching currents for JJs in the array can be written as, $I_s(n) \simeq I_s^* + \sigma(n/N - 1/2)$, where I_s^* is the mean switching current and σ is the width of the switching current distribution. At the optimal bias, $I_b \simeq I_s^*$, the effective differential resistance is, $R_d \simeq NV_c/\sigma$. The response of SCD is $\Delta V \simeq R_d I_{\text{THz}}$, where I_{THz} is the induced THz current. The absorbed THz power can be written as, $P_{\text{THz}} = I_{\text{THz}}^2 R_{\text{THz}}/2$, where R_{THz} is the real part of the high-frequency impedance of the detector (including electrodes). Thus, we obtain

$$S \simeq \frac{2NV_c}{\sigma R_{\text{THz}} I_{\text{THz}}}. \quad (1)$$

The procedure for quantitative estimation of sensitivity and noise-equivalent power (NEP) is described in Methods. For the case of Bi-2212 detectors from Figs. 2 and 3 we get $S > 10^7$ (V/W) and $NEP \sim 10^{-17}$ (W/ \sqrt{Hz}) for both MW and THz detection. There are very good numbers, however, far from optimal. Let's estimate achievable characteristics for a small, high-quality Bi-2212 mesa, like in Fig. 2 (c). Assuming $N = 500$, $V_c = 20$, $I_s^* = 50 \mu\text{A}$; $\sigma = 0.01 I_s^*$ (typical for fluctuation-induced σ at $T \sim 4$ K [8, 49]); $R_{\text{THz}} = 100 \Omega$ (for an efficient detector R_{THz} should be comparable to the impedance of free space); and $I_{\text{THz}} = 0.1\sigma = 50$ nA; we obtain $S \simeq 8 \cdot 10^{12}$ (V/W) and $NEP \simeq 10^{-22}$ (W/ \sqrt{Hz}). This estimation is made under realistic assumptions and does not represent the ultimate limit of SCD [8].

Two factors contribute to this high sensitivity: the large cascade gain N and the narrow switching width σ . The latter depends on the uniformity of the array, inter-junction coupling, thermal fluctuations and electrical noise. When all junction in the stack are identical, they will switch at the same bias current. A spread of parameters cause broadening of σ . However, coupling between JJs leads to current-locking even of slightly dissimilar junctions [36]. The true phase-locking of JJs can further reduce σ [51]. Therefore, a strong inter-junction coupling is crucial for such a detector. Ultimately, σ is limited by quantum fluctuations [14, 16–18, 24, 49], qualifying SCD as a quantum-limited photon detector.

A good detector should possess both high sensitivity to absorbed power and high absorption efficiency of incident radiation. The maximum efficiency (50%) is achieved at the impedance matching condition [39–41]. However, a single JJ alone cannot provide proper matching because it is much smaller than λ_0 [39]. Therefore, the geometry of electrodes forming a receiving antenna becomes crucial. In the case of linear Nb arrays, long electrodes function as traveling wave antennas, as evidenced by off-axis directivities of both emission [45, 46] and absorp-

tion, Fig. 1 (f). Whisker-based Bi-2212 mesas have a turnstile antenna geometry [35], Fig. 2(b), enabling high radiation efficiency (12% at $f \simeq 4$ THz) [22] and causing the four-fold receiving directivity, Fig. 2 (f) [50]. Thus, the analysis of directivity (geometry-specific antenna effects) provides a valuable tool for investigating impedance matching and the efficiency of both absorption and emission.

In conclusion, we have described the operational principle of a cascade switching current detector, utilizing arrays of coupled Josephson junctions. Coupling between junctions leads to the current locking phenomenon and results in avalanche-like switching of many junctions. This amplifies the readout voltage and enhances detector sensitivity. We have demonstrated two prototypes based either on low- T_c linear Nb arrays, or high- T_c stacked intrinsic Josephson junctions. Good impedance matching and absorption efficiency of the studied devices is confirmed by observation of geometry-specific antenna effects in receiving directivities. We conclude that Bi-2212 whisker-based cascade SCD are promising candidates for broad-band and high-performance THz sensors.

METHODS

Quantitative estimation of detector characteristics

For MW measurements the detector sensitivity is estimated as follows. First, the arriving MW power is measured using a cryostat as a bolometer. The sample stage in our cryostat has an effective thermal resistance $R_{th} \simeq 0.5$ K/mW [22]. By measuring a small temperature rise, $\Delta T \sim$ mK, caused by the MW beam we directly measure the total arriving power, $P_{tot} = \Delta T/R_{th}$. Because of the large $\lambda_0 \simeq 4$ mm and significant diffraction at several narrow (~ 1 cm) apertures of the cryostat, the power is fairly uniformly distributed over the sample space with the radius $r \sim 1.5$ cm and the mean power density $q_{MW} = P_{tot}/\pi r^2$. The incoming power on the device is then calculated as $P_{MW} = q_{MW}A$, assuming that $A = 1$ mm² is the effective absorption area of the receiving antenna, formed by the electrodes. For the case

of Fig. 2, $P_{tot} \simeq 10$ μ W and $P_{MW} \simeq 14$ nW.

The absorbed power, P_a , can be estimated from the suppression of the switching current, ΔI_s , caused by the generated high-frequency current. In the MW case (low frequency limit) ΔI_s is just equal to the induced MW current [8]. P_a is calculated using Eq. (4) from Ref. [19]: $P_a \simeq (2\sqrt{2}/3\pi)(\Delta I_s/I_{c0})^{3/2}I_{c0}V_c$. For the case of Fig. 2 (d), $\Delta I_s \simeq 3$ μ A at the attenuation 3.7 dB, $I_{c0} = 38$ μ A, $V_c = 20$ mV, yielding $P_a \simeq 5$ nW, approximately 30% of P_{MW} . The maximum voltage is $V \simeq 0.37$ V, and the sensitivity with respect to the absorbed power, $S_a = V/P_a \simeq 7.4 \cdot 10^7$ (V/W) and the net sensitivity $S_{MW} = V/P_{MW} \simeq 2.6 \cdot 10^7$ (V/W).

For THz generation-detection test in Fig. 3 we can not confidently estimate the incoming power. However, the absorbed power can be estimated in the same way. For the green I - V in Fig. 3 (e) at $V_{gen} = 2.65$ V, $f_J = 7.99$ THz, the suppression of switching current is $\Delta I_s = 35$ μ A. With $I_{c0} = 385$ μ A, $V_c = 20$ mV and $V \simeq 1$ V it yields $P_a \simeq 60$ nW and $S_a \simeq 1.6 \cdot 10^7$ (V/W).

The noise-equivalent power is determined as $NEP = v_n/S$, where v_n is the voltage noise. It is typically in the range of few nV/ \sqrt{Hz} at room temperature, but for lock-in measurements at low T it is certainly below 1 nV. Taking $v_n = 1$ nV/ \sqrt{Hz} we obtain the following values of NEP with respect to absorbed power: $NEP_{MW} \simeq 1.35 \cdot 10^{-17}$ W/ \sqrt{Hz} and $NEP_{THz} \simeq 6.25 \cdot 10^{-17}$ W/ \sqrt{Hz} .

The achieved characteristics are very good, but far from optimal, as discussed above. The main reason for the larger NEP_{THz} than NEP_{MW} is that the mesa used for the THz test has a factor 10 larger I_{c0} . The NEP of SCD is approximately proportional to the Josephson energy, $E_J = (\Phi_0/2\pi)I_{c0}$ [8]. Therefore, the weighted (by E_J) THz sensitivity is actually twice better than for MW.

Acknowledgements

The work was supported by the Science for Peace and Security Programme, grant G5796. We are grateful to R. Gerda and M. Galin for assistance with the fabrication of Nb-arrays and to A. Kalenyuk and E. Borodianskyi for assistance with the fabrication of Bi-2212 samples.

-
- [1] M. Zhang and J.T.W. Yeow, Nanotechnology-Based Terahertz Biological Sensing. *IEEE Nanotechn. Mag.* **10**, 30 (2016).
 - [2] R. A. Lewis, A review of terahertz detectors. *J. Phys. D: Appl. Phys.* **52**, 433001 (2019).
 - [3] S. R. Kasjoo, M. B. Mohd Mokhar, N. F. Zakaria and N. J. Juhari, A brief overview of detectors used for terahertz imaging systems. *AIP Conf. Proc.* **2203**, 020020 (2020).
 - [4] M. D. Eisaman, J. Fan, A. Migdall, and S. V. Polyakov. Invited Review Article: Single-photon sources and detectors. *Rev. Sci. Instrum.* **82**, 071101 (2011).
 - [5] S. Komiyama, O. Astafiev, V. Antonov, T. Kutsuwa, and H. Hirai, A single-photon detector in the far-infrared range. *Nature* **403**, 405 (2000).
 - [6] G. Auton, D. B. But, J. Zhang, E. Hill, D. Coquillat, C. Consejo, P. Nouvel, W. Knap, L. Varani, F. Teppe, J. Torres, and A. Song, Terahertz Detection and Imaging Using Graphene Ballistic Rectifiers. *Nano Lett.* **17**, 7015 (2017).
 - [7] J. A. Lau, V. B. Verma, D. Schwarzer, and A. M. Wodtke, Superconducting single-photon detectors in the mid-infrared for physical chemistry and spectroscopy.

- Chem. Soc. Rev.* **52**, 921 (2023).
- [8] V. M. Krasnov. Resonant switching current detector based on underdamped Josephson junctions. *arXiv:2403.03803* (2024).
- [9] C. C. Grimes, P. L. Richards, S. Shapiro. Josephson-Effect Far-Infrared Detector. *J. Appl. Phys.* **39**, 3905–3912 (1968).
- [10] H. Kanter, F. L. Vernon, Jr. High-Frequency Response of Josephson Point Contacts. *J. Appl. Phys.* **43**, 3174–3183 (1972).
- [11] A.N. Vystavkin, V.N. Gubankov, L.S. Kuzmin, K.K. Likharev, V.V. Migulin, V.K. Semenov. S-c-S junctions as nonlinear elements of microwave receiving devices. *Rev. de Physique Appl.* **9**, 79-109 (1974).
- [12] J. R. Tucker, M. J. Feldman. Quantum detection at millimeter wavelengths. *Rev. Mod. Phys.* **57**, 1055 (1985).
- [13] N. Grønbech-Jensen, M. G. Castellano, F. Chiarello, M. Cirillo, C. Cosmelli, L.V. Filippenko, R. Russo, and G. Torrioli. Microwave-Induced Thermal Escape in Josephson Junctions. *Phys. Rev. Lett.* **93**, 1007002 (2004).
- [14] A. Poudel, R. McDermott, and M. G. Vavilov. Quantum efficiency of a microwave photon detector based on a current-biased Josephson junction. *Phys. Rev. B* **86**, 174506 (2012).
- [15] G. Oelsner, L. S. Revin; E. Il'ichev, A. L. Pankratov, H.-G. Meyer, L. Grönberg, J. Hassel, and L. S. Kuzmin. Underdamped Josephson junction as a switching current detector. *Appl. Phys. Lett.* **103**, 142605 (2013).
- [16] C. K. Andersen, and K. Mølmer. Effective description of tunneling in a time-dependent potential with applications to voltage switching in Josephson junctions. *Phys. Rev. A* **87**, 052119 (2013).
- [17] K. Inomata, Z. Lin, K. Koshino, W. D. Oliver, J.-S. Tsai, T. Yamamoto, and Y. Nakamura. Single microwave-photon detector using an artificial Λ -type three-level system. *Nature Commun.* **7**, 12303 (2016).
- [18] G. Oelsner, C. K. Andersen, M. Reháč, M. Schmelz, S. Anders, M. Grajcar, U. Hübner, K. Mølmer, and E. Il'ichev. Detection of Weak Microwave Fields with an Underdamped Josephson Junction. *Phys. Rev. Appl.* **7**, 014012 (2017).
- [19] E. A. Borodianskyi and V. M. Krasnov, Josephson emission with frequency span 1-11 THz from small $\text{Bi}_2\text{Sr}_2\text{CaCu}_2\text{O}_{8+\delta}$ mesa structures, *Nat. Commun.* **8**, 1742 (2017).
- [20] L. S. Revin, A. L. Pankratov, A. V. Gordeeva, A. A. Yablokov, I. V. Rakut, V. O. Zbrozhek, and L. S. Kuzmin. Microwave photon detection by an Al Josephson junction. *Beilstein J. Nanotechnol.* **11**, 960–965 (2020).
- [21] V. V. Pavlovskiy, I. I. Gundareva, O. Y. Volkov, Y. Y. Divin. Wideband detection of electromagnetic signals by high- T_c Josephson junctions with comparable Josephson and thermal energies. *Appl. Phys. Lett.* **116**, 082601 (2020).
- [22] R. Cattaneo, E. A. Borodianskyi, A. A. Kalenyuk, and V. M. Krasnov, Superconducting Terahertz Sources with 12% Power Efficiency. *Phys. Rev. Appl.* **16**, L061001 (2021).
- [23] F. Chiarello, et al., Investigation of Resonant Activation in a Josephson Junction for Axion Search With Microwave Single Photon Detection. *IEEE Trans. Appl. Supercond.* **32**, 1100305 (2022).
- [24] I. A. Devyatov, L. S. Kuzmin, K. K. Likharev, V. V. Migulin, A. B. Zorin. Quantum-statistical theory of microwave detection using superconducting tunnel junctions. *J. Appl. Phys.* **60**, 1808-1828 (1986).
- [25] S. O. Katterwe, H. Motzkau, A. Rydh, and V. M. Krasnov. Coherent generation of phonon-polaritons in $\text{Bi}_2\text{Sr}_2\text{CaCu}_2\text{O}_{8+x}$ intrinsic Josephson junctions. *Phys. Rev. B* **83**, 100510(R) (2011).
- [26] V. M. Krasnov. Interlayer tunneling spectroscopy of $\text{Bi}_2\text{Sr}_2\text{CaCu}_2\text{O}_{8+\delta}$: A look from inside on the doping phase diagram of high- T_c superconductors. *Phys. Rev. B* **65**, 140504(R) (2002).
- [27] V. M. Krasnov. Temperature dependence of the bulk energy gap in underdoped $\text{Bi}_2\text{Sr}_2\text{CaCu}_2\text{O}_{8+\delta}$: Evidence for the mean-field superconducting transition. *Phys. Rev. B* **79**, 214510 (2009).
- [28] R. Kleiner and P. Müller, Intrinsic Josephson effects in high- T_c superconductors. *Phys. Rev. B* **49**, 1327 (1994).
- [29] L. Ozyuzer, A. E. Koshelev, C. Kurter, N. Gopalsami, Q. Li, M. Tachiki, K. Kadowaki, T. Yamamoto, H. Minami, H. Yamaguchi, T. Tachiki, K. E. Gray, W.-K. Kwok, and U. Welp, Emission of Coherent THz Radiation from Superconductors. *Science* **318**, 1291 (2007).
- [30] T. M. Benseman, K. E. Gray, A. E. Koshelev, W.-K. Kwok, U. Welp, H. Minami, K. Kadowaki, and T. Yamamoto, Powerful terahertz emission from $\text{Bi}_2\text{Sr}_2\text{CaCu}_2\text{O}_{8+\delta}$ mesa arrays. *Appl. Phys. Lett.* **103**, 022602 (2013).
- [31] T. Kashiwagi, T. Yamamoto, H. Minami, M. Tsujimoto, R. Yoshizaki, K. Delfanazari, T. Kitamura, C. Watanabe, K. Nakade, T. Yasui, K. Asanuma, Y. Saiwai, Y. Shibano, T. Enomoto, H. Kubo, K. Sakamoto, T. Katsuragawa, B. Marković, J. Mirković, R. A. Klemm, and K. Kadowaki, Efficient Fabrication of Intrinsic-Josephson-Junction Terahertz Oscillators with Greatly Reduced Self-Heating Effects. *Phys. Rev. Appl.* **4**, 054018 (2015).
- [32] H. Zhang, R. Wieland, W. Chen, O. Kizilaslan, S. Ishida, C. Han, W. Tian, Z. Xu, Z. Qi, T. Qing, Y. Lv, X. Zhou, N. Kinev, A. B. Ermakov, E. Dorsch, M. Ziegele, D. Koelle, H. Eisaki, Y. Yoshida, V. P. Koshelets, R. Kleiner, H. Wang, and P. Wu, Resonant Cavity Modes in $\text{Bi}_2\text{Sr}_2\text{CaCu}_2\text{O}_{8+x}$ Intrinsic Josephson Junction Stacks, *Phys. Rev. Appl.* **11**, 044004 (2019).
- [33] Y. Ono, H. Minami, G. Kuwano, T. Kashiwagi, M. Tsujimoto, K. Kadowaki, R. A. Klemm. Superconducting Emitter Powered at 1.5 Terahertz by an External Resonator. *Phys. Rev. Appl.* **13**, 064026 (2020).
- [34] M. Miyamoto, R. Kobayashi, G. Kuwano, M. Tsujimoto, and I. Takeya, Wide-band frequency modulation of a terahertz intrinsic Josephson junction emitter of a cuprate superconductor. *Nat. Photon.* (2024). <https://doi.org/10.1038/s41566-023-01348-0>.
- [35] M. M. Krasnov, N. D. Novikova, R. Cattaneo, A. A. Kalenyuk and V. M. Krasnov, Design aspects of $\text{Bi}_2\text{Sr}_2\text{CaCu}_2\text{O}_{8+\delta}$ THz sources: optimization of thermal and radiative properties. *Beilstein J. Nanotechnol.* **12**, 1392 (2021).
- [36] S. Yu. Grebenchuk, R. Cattaneo, and V. M. Krasnov. Nonlocal Long-Range Synchronization of Planar Josephson-Junction Arrays. *Phys. Rev. Appl.* **17**, 064032 (2022).
- [37] T. Golod, O. M. Kapran and V. M. Krasnov. Planar Superconductor-Ferromagnet-Superconductor Josephson Junctions as Scanning-Probe Sensors. *Phys. Rev. Appl.* **11**, 014062 (2019).

- [38] J. C. LeFebvre, E. Cho, H. Li, K. Pratt, and S. A. Cybart, Series arrays of planar long Josephson junctions for high dynamic range magnetic flux detection. *AIP Adv.* **9**, 105215 (2019).
- [39] V. M. Krasnov, A distributed active patch antenna model of a Josephson oscillator. *Beilstein J. Nanotechnol.* **14**, 151 (2023).
- [40] V. M. Krasnov, Coherent flux-flow emission from stacked Josephson junctions: Nonlocal radiative boundary conditions and the role of geometrical resonances. *Phys. Rev. B* **82**, 134524 (2010).
- [41] C.A. Balanis, Antenna Theory: Analysis and Design, 3rd ed.; John Wiley & Sons, Inc., Publ.: Hoboken, New Jersey, 2005.
- [42] W. R. McCrath, A. V. Räisänen, and P. L. Richards. Accurate Noise Measurements of Superconducting Quasiparticle Array Mixers. *IEEE Trans. Magn.* **21**, 212 (1985).
- [43] S. V. Shitov, V. P. Koshelets, S. A. Kovtonyuk, A. B. Ermakov, N. D. Whyborn and C.-O. Lindström, Ultra-low-noise 100 GHz receiver based on parallel biased SIS arrays. *Supercond. Sci. Techn.* **4**, 406 (1991).
- [44] F. Mueller, R. Behr, T. Weimann, L. Palafox, D. Olaya, P. D. Dresselhaus and S. P. Benz, 1 V and 10 V SNS Programmable Voltage Standards for 70 GHz. *IEEE Trans. Appl. Supercond.* **19**, 3, 981-986 (2009)
- [45] M. A. Galin, E. A. Borodianskyi, V. V. Kurin, I. A. Shereshevskiy, N. K. Vdovicheva, V. M. Krasnov, and A. M. Klushin. Synchronization of Large Josephson-Junction Arrays by Traveling Electromagnetic Waves. *Phys. Rev. Appl.* **9**, 054032 (2018).
- [46] M. A. Galin, F. Rudau, E. A. Borodianskyi, V.V. Kurin, D. Koelle, R. Kleiner, V.M. Krasnov, and A.M. Klushin. Direct Visualization of Phase-Locking of Large Josephson Junction Arrays by Surface Electromagnetic Waves. *Phys. Rev. Appl.* **14**, 024051 (2020).
- [47] R. Cattaneo, M. A. Galin and V.M. Krasnov. Observation of collective excitation of surface plasmon resonances in large Josephson junction arrays. *Beilstein J. Nanotechnol.* **13**, 1578–1588 (2022).
- [48] V. M. Krasnov, S.-O. Katterwe, and A. Rydh, Signatures of the electronic nature of pairing in high-Tc superconductors obtained by non-equilibrium boson spectroscopy. *Nature Commun.* **4**, 2970 (2013).
- [49] V. M. Krasnov, T. Bauch, S. Intiso, E. Hürfeld, T. Akazaki, H. Takayanagi, and P. Delsing. Collapse of Thermal Activation in Moderately Damped Josephson Junctions. *Phys. Rev. Lett.* **95**, 157002 (2005).
- [50] The directivity of turnstile antenna depends on the phase shift between two dipoles, which we can not control, and on the mode number. Therefore, there could be a large variety of directivities, see e.g. [41]. Nevertheless, the observed four-fold polarization dependence is a clear evidence for the geometry-related antenna effect.
- [51] N. Mros, V.M. Krasnov, A. Yurgens, D. Winkler and T. Claeson, Multiple-valued c-axis critical current and phase locking in $\text{Bi}_2\text{Sr}_2\text{CaCu}_2\text{O}_{8+\delta}$ single crystals. *Phys. Rev. B* **57**, R8135 (1998).